Large Arrays and Properties of 3-Terminal Graphene Nanoelectromechanical Switches

*Xinghui Liu, Ji Won Suk, Narasimha G. Boddeti, Lauren Cantley, Luda Wang, Jason M. Gray, Harris J. Hall, Victor M. Bright, Charles T. Rogers, Martin L. Dunn, Rodney S. Ruoff, and J. Scott Bunch**

Nanoelectromechanical (NEMS) switches are promising devices used for mechanical computing, data storage, and RF communication,[1–7] due to their attractive attributes such as microwave operating frequencies, low power consumption, high on/off ratio, radiation hardness, and device density comparable to semiconductor integrated circuits.[8–14] Graphene, an atomic sheet of graphite, is the thinnest and strongest material in the world.[15,16] Its high Young's modulus (1 TPa), extremely low mass (only 1 layer of atoms), and low resistivity (1 μΩ-cm), makes it an ideal material for a NEMS switch.[11,14,17–22] Previously reported graphene based NEMS switches are primarily 2-terminal, one-off laboratory scale demonstrations.[11,14,21,23] These switches operate by deflecting a suspended graphene membrane with a source-drain voltage (V_{sd}) and measuring the current once contact is made. A 3-terminal NEMS switch, on the other hand, using a third electrode to apply an actuation voltage (V_g) independent of the V_{sd}, provides further advantages such as greater operational flexibility, lower power consumption, and higher level of integration and system functionality compared to 2-terminal devices.[24–26] The graphene contact switches reported to date are primarily doubly clamped beams that suffer reliability problems due to tears on open edges and/or irreversible stiction of graphene.[11,14] Here, we fabricate and characterize a large array of circularly clamped graphene NEMS switches, which can work with either 2-terminal or 3-terminal electromechanical switching. The devices show low actuation voltage and improved mechanical integrity with a novel design, which also reduces the contact area thereby reducing stiction problems.

The graphene NEMS switch array is made by a bottom-up fabrication process.[3] We start with a substrate (typically 2 cm × 1 cm) which includes prefabricated gold electrodes defining source and drain electrodes, a doped silicon layer which acts as a gate electrode, and predefined wells over which suspended graphene is transferred (**Figure 1**a) (see Supporting Information). Each chip which will contain ~1000 devices is separated into individual units (~700 μm × 700 μm) by trenches etched through the device silicon layer on which source electrodes are deposited, and each unit is prepared with four drain electrodes that correspond to a single source electrode. Finally, monolayer graphene films are grown by chemical vapor deposition (CVD) on copper, patterned into rectangular strips, and then transferred to the prefabricated substrates using a dry transfer technique.[27,28] Figure 1c is an optical image of a completed device. Atomic force microscope (AFM) images of suspended graphene membranes were taken for more than 100 devices with a Veeco Dimension 3100 in non-contact mode (tip: μmasch, mode NSC15, 325 kHz, 46 N m^{-1}), and the majority of initial deflections before electrical measurements at room temperature and atmosphere are between 50–100 nm downward. (see statistical distribution of the initial deflections in Supporting Information). This initial deflection was found to increase after electrical measurements were performed suggesting that further slack is introduced in the graphene, presumably through sliding of the graphene. Figure 1d is an example of the AFM image of the switch showing graphene suspended over the etched well and electrically contacting the drain electrode. A side view schematic of the completed device is shown in Figure 1b. A monolayer graphene film is electrically contacted to a drain electrode and suspended over a gate and source electrode (all of which are electrically isolated from each other.)

The completed device can work either as a two-terminal or three-terminal NEMS switch. All the electrical measurements are performed at 78 K and a pressure of ~10^{-6} Torr unless otherwise indicated to eliminate the influence of capillary forces due to adsorbed water on device operation. The low temperature electrical measurements in vacuum are measured in a Desert cryogenic probe station cooled by liquid nitrogen. In 2-terminal operation, a voltage between the source and drain electrodes, V_{sd}, is used to electrostatically deflect the graphene membrane. When the graphene membrane gets sufficiently close to the source electrode it forms a conducting pathway

X. Liu, N. G. Boddeti, L. Cantley, L. Wang, Dr. J. M. Gray, Dr. H. J. Hall, Prof. V. M. Bright, Prof. J. S. Bunch
Department of Mechanical Engineering
University of Colorado, Boulder, CO, 80309, USA
E-mail: bunch@bu.edu
Prof. J. S. Bunch
Department of Mechanical Engineering
Boston University
Boston, MA, 02215, USA and Division of Materials Science and Engineering, Boston, University, Brookline, Massachusetts 02446, USA
Dr. J. Won Suk, Prof. R. S. Ruoff
Department of Mechanical Engineering and
the Materials Science and Engineering Program
The University of Texas
Austin, TX, 78712, USA
Prof. C. T. Rogers
Department of Physics
University of Colorado
Boulder, CO, 80309, USA
Prof. M. L. Dunn
Singapore University of Technology and Design
Singapore, 138682

DOI: 10.1002/adma.201304949

© 2013 WILEY-VCH Verlag GmbH & Co. KGaA, Weinheim

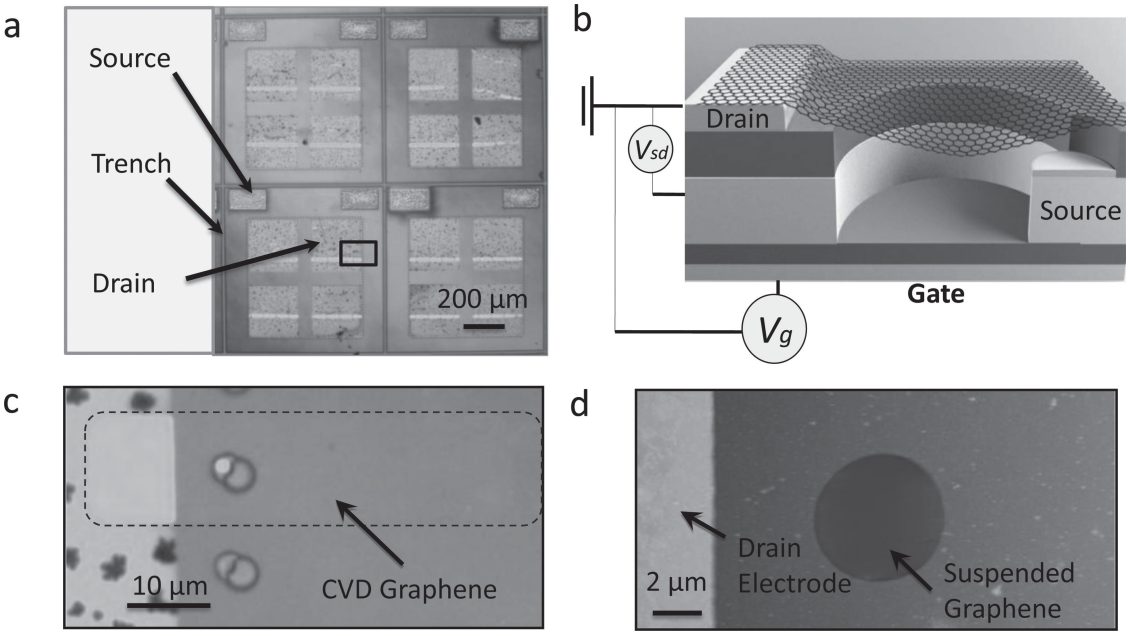

Figure 1. Device design and fabrication a) Optical image of a four unit array of graphene NEMS switches. b) Three dimensional schematic of a 3-terminal graphene NEMS switch. c) Zoomed in optical image of a single graphene NEMS switch located in the black rectangle in (a). d) Atomic force microscope image of a graphene NEMS switch.

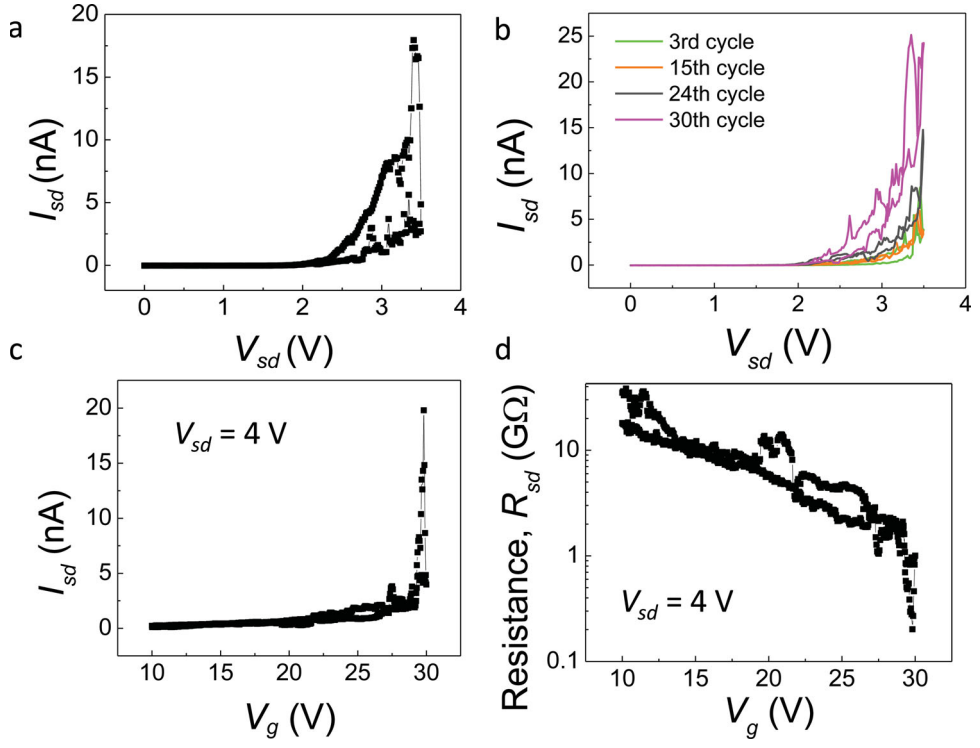

Figure 2. Electrical characterization of graphene NEMS switches a) Current, I_{sd}, vs source-drain voltage, V_{sd}, for a graphene NEMS switch under two-terminal switching with the gate voltage $V_g = 0$. A trace and retrace is shown. b) Current, I_{sd}, vs source-drain voltage, V_{sd}, for the same graphene NEMS switch in (a) under multiple two-terminal switching with the gate voltage $V_g = 0$. A trace and retrace is shown for each cycle. c) Current, I_{sd}, vs gate voltage, V_g, for a graphene NEMS switch operated as a 3-terminal switch where $V_{sd} = 4$ V. A trace and retrace is shown. d) Resistance, R_{sd}, vs V_g for the same trace shown in (c).

© 2013 WILEY-VCH Verlag GmbH & Co. KGaA, Weinheim
Adv. Mater. **2013**,
DOI: 10.1002/adma.201304949

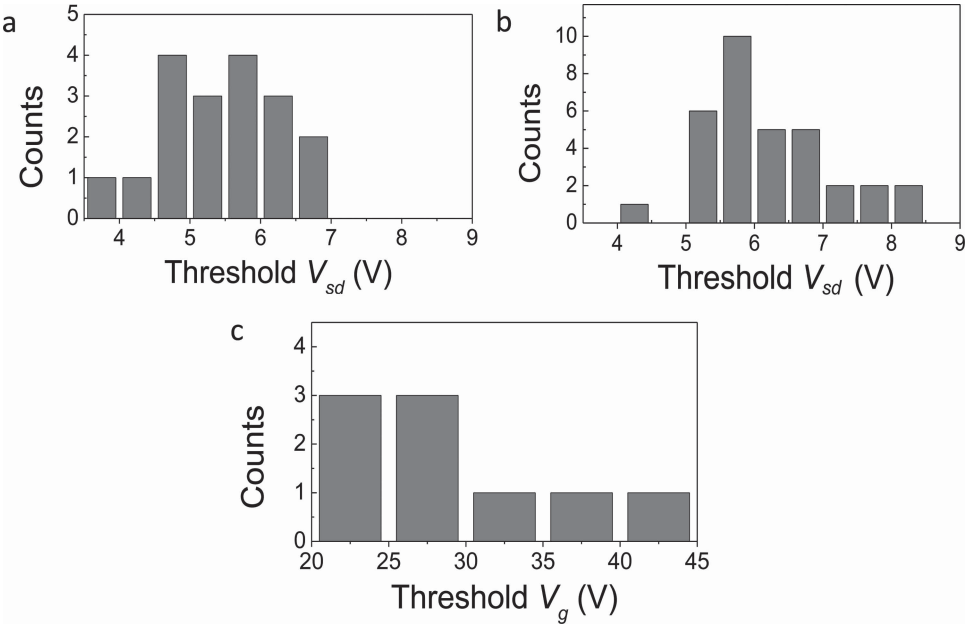

Figure 3. Statistical distribution of threshold switching voltages a) A histogram showing the number of devices vs their respective switching voltage for 2-terminal graphene NEMS switches with d_1 = 120 nm. The average and standard deviation threshold V_{sd} = 5.45 ± 0.85 V. b) A histogram showing the number of devices vs their respective switching voltage for 2-terminal graphene NEMS switches with d_1 = 160 nm. The average and standard deviation threshold V_{sd} = 6.23 ± 0.89 V. c) A histogram showing the number of devices vs their respective switching voltage for 3-terminal graphene NEMS switches with d_1 = 120 nm and V_{sd} = 3 V.

between the source and drain electrode which results in a current, I_{sd} (**Figure 2**a). In 2-terminal operation the gate voltage is kept at V_g = 0. At a critical voltage of V_{sd} ~ 3.5 V, the current between the source and drain electrodes increases abruptly and the device switches "on"; when V_{sd} is swept back to 0V the current abruptly decreases which leads to the "off" position. The typical number of switching cycles measured is ~ 10–30. Figure 2b shows the same device switching up to 30 times. There is some small scatter in the switching voltage but most of the switching takes place between V_{sd} ~ 3.0 V– 3.5 V.

In 3-terminal operation, a constant V_{sd} is applied and then the gate voltage is swept until switching commences. Data for a different graphene switch is shown in Figure 2c. The device switches at V_g ~ 30 V, with V_{sd} = 4 V. Figure 2d shows the corresponding resistance, R_{sd}, vs V_g for the same device. Initially the "off state" has a high resistance ~10 GΩ. As the gate voltage is increased, there is an electrostatic force on the graphene membrane that pulls the graphene closer to the drain electrode. This is supported by the resistance decreasing with V_g, suggesting some tunnelling or leakage current between the graphene and drain electrode. At V_g ~30 V, the graphene is sufficiently close to the drain electrode that more intimate contact is made and the R decreases by ~1 order of magnitude. Both the 2-terminal and 3-terminal switching I-V curves follow a similar behavior to other previously reported NEMS switches where the current increases gradually at first following a smooth curve, and then increases abruptly.[6,11,14,24] For both the 2-terminal and 3-terminal switches, we define the voltage at the point when the current starts to jump as the "threshold voltage".

The design of our graphene NEMS contact switch is different from that of most traditional MEMS/NEMS switches, in which a doubly clamped beam or cantilever makes large area surface contact with an electrode.[2,6,7,11,14,23,24,29] Our device switches with a "line" contact similar to a recently reported "pipe clip" geometry.[13] A distinct advantage of this geometry is that tear is eliminated and stiction is limited, which addresses two major challenges facing implementation of a reliable graphene NEMS switch. Furthermore, in the design, the graphene membrane with its edge completely clamped provides higher restoring force compared with a doubly clamped beam or cantilever structure of the same dimensions.[11,14] From more than one hundred devices scanned with non-contact mode AFM before and after switching, no tears in the graphene membrane have been observed. In addition, this design with the graphene membrane making a "line" contact also decreases the contact area, which provides a platform to reduce stiction problems.[11,13,30,31]

We measured the threshold V_{sd} in 51 2-terminal devices with the same geometry and dimensions (radius of cavities a = 2.5 μm, radius of source electrodes b = 1 μm) but varied the separation between graphene and source electrodes, d_1 (**Figure 3**a and 3b). The average threshold voltage V_{sd} and standard deviation are 5.45 ± 0.85 V for devices with d_1 = 120 nm (Figure 3a), and 6.23 ± 0.89 V for d_1 = 160 nm (Figure 3b), respectively. This decrease in the average threshold V_{sd} is consistent with the simple electrostatic model where decreasing d_1 leads to a decreasing threshold V_{sd}. The measured threshold V_{sd} is as low as 3.5 V, and all of them are less than 10 V. These low voltages are much smaller than typical MEMS switches (30 – 50 V) and comparable to CMOS logic and conventional dynamic random access memory (RAM) technology.[8,29] We also measured 9 3-terminal graphene switches, and the threshold V_g ranges from 20 V to 45 V, while V_{sd} is set as 3 V (Figure 3c).

© 2013 WILEY-VCH Verlag GmbH & Co. KGaA, Weinheim

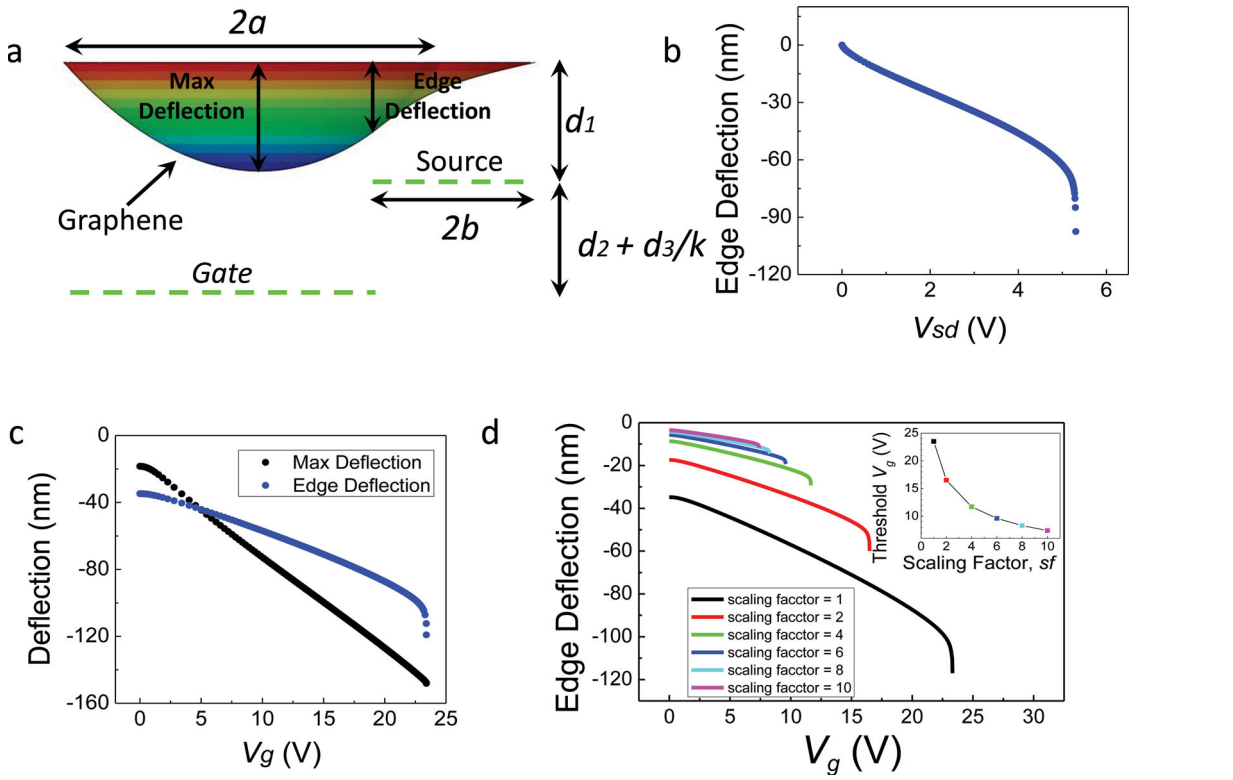

Figure 4. Theoretical modeling of switching a) Simulation of the graphene NEMS switch. b) Simulation results showing the edge deflection vs V_{sd} of graphene switches (a = 2.5 µm, b = 1 µm, d_1 = 120 nm, d_2 = 230 nm, d_3 = 200 nm), assuming effective Young's modulus E_{eff} = 0.4 TPa, Poisson's ratio ν = 0.16 and thickness t = 0.34 nm. c) Simulation results showing the pull-in of three terminal graphene switches with the same geometry dimension as (b) assuming effective Young's modulus E_{eff} = 0.4 TPa, Poisson's ratio ν = 0.16 and thickness t = 0.34 nm. V_{sd} = 3 V. d) Simulation results showing plot of edge deflection vs V_g with scaling factor = 1–10. Inset is the plot of threshold V_{sd} vs scaling factor, *sf*.

To understand the mechanics of the switches, we numerically model our device using non-linear finite element simulations with the software package Abaqus (see Supporting Information). We use a decoupled electro-mechanical model that approximates the electrostatic force at a point (*x*,*y*) on the deformable electrode to be the same as that between two parallel plates and this approach gives a reasonable approximate solution (**Figure 4**a).[32–34] The electrostatic pressure from the gate electrode P_g and source electrode P_{sd} on the graphene membrane are defined as follows.

$$P_g = \frac{\varepsilon_0 V_g^2}{2\left(d_1 + d_2 + d_3/k - w(x,y)\right)^2} \quad (1)$$

$$P_{sd} = \frac{\varepsilon_0 V_{sd}^2}{2\left(d_1 - w(x,y)\right)^2} \quad (2)$$

where, d_2, d_3 are the initial separations between source and box oxide layer, and the thickness of the box oxide layer, ε_0 is the dielectric permittivity of vacuum space, κ (= 3.9) is dielectric constant of silicon dioxide,[35] while $w(x,y)$ gives the deflection of the graphene membrane as function of the x and y coordinates. The electrostatic pressure P_g and P_{sd} act on regions of the graphene directly above the gate and drain electrodes respectively. An example of the simulation results for 2-terminal and 3-terminal configurations are shown in Figure 4b and Figure 4c, respectively assuming the effective Young's modulus of CVD graphene E_{eff} = 0.4 TPa, which is about 40% of the Young's modulus of exfoliated monolayer graphene but is reasonably close to a recently reported value for CVD graphene.[36] The geometrical dimensions are: a = 2.5 µm, b = 1 µm, d_1 = 120 nm, d_2 = 230 nm and d_3 = 200 nm. In the finite element simulations of 2-terminal switching, V_{sd} is varied continuously until the membrane is pulled-in,[37,38] which is shown by an abrupt drop in the deflection of graphene membrane above the edge of source electrode as defined in Figure 4a. For the simulation of 3-terminal operation of devices with the same dimensions, V_{sd} is fixed at 3 V and V_g is varied until the graphene membrane is pulled into contact with the source electrode. The threshold V_{sd} and V_g obtained from the simulations are 5.3 V and 23.4 V, respectively. Using the finite element simulations, we took E_{eff} to be a fitting parameter and derived a distribution of E_{eff} from the data shown in Figure 3. To fit the data in Figure 3a and 3c, an average value of E_{eff} = 0.4 TPa is required, while an average of E_{eff} = 0.15 TPa for the data in Figure 3b. We think the scatter and deviation in the data of threshold voltages are caused by wrinkles or slack, both initial slack in the transferred graphene and slack introduced through sliding caused by the electrostatic actuation; furthermore, the range of E_{eff} is in line with reported values from CVD graphene.[36] Further detailed studies of the deformation mechanisms would be needed to

© 2013 WILEY-VCH Verlag GmbH & Co. KGaA, Weinheim
Adv. Mater. **2013**,
DOI: 10.1002/adma.201304949

conclusively resolve these uncertainties, but the overall behaviour appears to be adequately described by the model with the modulus adjusted to account for various potential softening mechanisms.[36]

The threshold voltages for our 3-terminal switches range from 20 V to 45 V. However, we find that the value decreases by further scaling down the dimension of the devices in a study of scaling effects with finite element simulations similar to previous ones. We scaled down all the dimensions (initial dimensions: a = 2.5 μm, b = 1 μm, d_1 = 120 nm, d_2 = 230 nm, d_3 = 200 nm) by the same scaling factor (*sf*) and did the simulations in the 3-terminal configuration. The results of these simulations, where the deformations scaled exactly with the inverse of the scaling factor, are shown through gate voltage (V_g) versus edge deflection plots in Figure 4d. The simulated threshold V_g decreased with *sf* increasing from 1 to 10. When the device is scaled down by 10 times (final dimensions with *sf* = 10: a = 250 nm, b = 100 nm, d_1 = 12 nm, d_2 = 23 nm, d_3 = 20 nm), the threshold V_g is found to be decreased to 7.4 V from 23.5 V with V_{sd} = 3 V, shown in the inset of Figure 4d. This indicates that we can potentially have larger device densities with lower actuation voltages and improved efficiencies just by scaling down the devices.

In conclusion, we fabricated and characterized a large array of graphene NEMS switches with a unique design, sub –5 V actuation, and an improved mechanical integrity of the graphene membranes. This design, with the graphene membrane having a "line" contact during switching, holds the promise to address the adhesion challenges in graphene nanomechanical switches. We also study the effect of scaling to the decrease of actuation voltage with simulation, thereby providing an instructive guide for further scaling of graphene NEMS switches.

Experimental Section

See detailed description of experimental materials and methods in the Supporting Information.

Supporting Information

Supporting Information is available from the Wiley Online Library or from the author.

Acknowledgements

This work was supported by NSF Grants #0900832(CMMI: Graphene Nanomechanics: The Role of van der Waals Forces), #1054406(CMMI: CAREER: Atomic Scale Defect Engineering in Graphene Membranes), the DARPA Center on Nanoscale Science and Technology for Integrated Micro/Nano-Electromechanical Transducers (iMINT), the National Science Foundation (NSF) Industry/University Cooperative Research Center for Membrane Science, Engineering and Technology (MAST), and in part by the NNIN and the National Science Foundation under Grant No. ECS-0335765.

Received: October 4, 2013
Published online:

[1] International Roadmap Committee Future Memory Devices Workshop Summary, **2010**.
[2] T. Rueckes, K. Kim, E. Joselevich, G. Y. Tseng, C.-L. Cheung, C. M. Lieber, *Science* **2000**, *289*, 94–97.
[3] W. Lu, C. M. Lieber, *Nat. Mater.* **2007**, *6*, 841–850.
[4] P. Gammel, G. Fischer, J. Bouchaud, *Bell Labs Technical Journal* **2005**, *10*, 29–59.
[5] W. Han, A. L. Hsu, T. Palacios, *Microwave Magazine, IEEE* **2012**, *13*, 114–125.
[6] A. B. Kaul, E. W. Wong, L. Epp, B. D. Hunt, *Nano Lett.* **2006**, *6*, 942–947.
[7] J. E. Jang, S. N. Cha, Y. J. Choi, D. J. Kang, T. P. Butler, D. G. Hasko, J. E. Jung, J. M. Kim, G. A. J. Amaratunga, *Nat. Nano* **2008**, *3*, 26–30.
[8] O. Y. Loh, H. D. Espinosa, *Nat. Nano* **2012**, *7*, 283–295.
[9] M. Liao, S. Hishita, E. Watanabe, S. Koizumi, Y. Koide, *Adv. Mater.* **2010**, *22*, 5393–5397.
[10] M. Roukes, *Physics World* **2001**, *14*, 25.
[11] Z. Shi, H. Lu, L. Zhang, R. Yang, Y. Wang, D. Liu, H. Guo, D. Shi, H. Gao, E. Wang, G. Zhang, *Nano Research* **2011**, *5*, 82–87.
[12] O. Loh, X. Wei, J. Sullivan, L. E. Ocola, R. Divan, H. D. Espinosa, *Adv. Mater.* **2012**, *24*, 2463–2468.
[13] J. O. Lee, Y.-H. Song, M.-W. Kim, M.-H. Kang, J.-S. Oh, H.-H. Yang, J.-B. Yoon, *Nat. Nano* **2013**, *8*, 36–40.
[14] K. M. Milaninia, M. A. Baldo, A. Reina, J. Kong, *Appl. Phys. Lett.* **2009**, *95*, 183105.
[15] A. K. Geim, *Science* **2009**, *324*, 1530–1534.
[16] A. K. Geim, K. S. Novoselov, *Nat. Mater.* **2007**, *6*, 183–191.
[17] J. S. Bunch, A. M. van der Zande, S. S. Verbridge, I. W. Frank, D. M. Tanenbaum, J. M. Parpia, H. G. Craighead, P. L. McEuen, *Science* **2007**, *315*, 490–493.
[18] C. Lee, X. Wei, J. W. Kysar, J. Hone, *Science* **2008**, *321*, 385–388.
[19] J. S. Bunch, S. S. Verbridge, J. S. Alden, A. M. van der Zande, J. M. Parpia, H. G. Craighead, P. L. McEuen, *Nano Lett.* **2008**, *8*, 2458–2462.
[20] K. S. Novoselov, A. K. Geim, S. V. Morozov, D. Jiang, Y. Zhang, S. V. Dubonos, I. V. Grigorieva, A. A. Firsov, *Science* **2004**, *306*, 666–669.
[21] S. M. Kim, E. B. Song, S. Lee, S. Seo, D. H. Seo, Y. Hwang, R. Candler, K. L. Wang, *Appl. Phys. Lett.* **2011**, *99*, 23103.
[22] B. Standley, W. Bao, H. Zhang, J. Bruck, C. N. Lau, M. Bockrath, *Nano Lett.* **2008**, *8*, 3345–3349.
[23] P. Li, Z. You, G. Haugstad, T. Cui, *Appl. Phys. Lett.* **2011**, *98*, 253103–253105.
[24] S. W. Lee, S. J. Park, E. E. B. Campbell, Y. W. Park, *Nat. Commun.* **2011**, *2*, 220.
[25] S. Chong, B. Lee, K. B. Parizi, J. Provine, S. Mitra, R. T. Howe, H.-S. P. Wong, *Electron Devices Meeting (IEDM), 2011 IEEE International* **2011**, 30.5.1–30.5.4.
[26] K. Akarvardar, D. Elata, R. Parsa, G. C. Wan, K. Yoo, J. Provine, P. Peumans, R. T. Howe, H. S. P. Wong, in *Electron Devices Meeting, 2007*. IEDM 2007. IEEE International, **2007**, pp. 299–302.
[27] X. Li, W. Cai, J. An, S. Kim, J. Nah, D. Yang, R. Piner, A. Velamakanni, I. Jung, E. Tutuc, S. K. Banerjee, L. Colombo, R. S. Ruoff, *Science* **2009**, *324*, 1312–1314.
[28] J. W. Suk, A. Kitt, C. W. Magnuson, Y. Hao, S. Ahmed, J. An, A. K. Swan, B. B. Goldberg, R. S. Ruoff, *ACS Nano* **2011**, *5*, 6916–6924.
[29] D. A. Czaplewski, G. A. Patrizi, G. M. Kraus, J. R. Wendt, C. D. Nordquist, S. L. Wolfley, M. S. Baker, M. P. de Boer, *J. Micromech. Microeng.* **2009**, *19*, 85003.
[30] S. P. Koenig, N. G. Boddeti, M. L. Dunn, J. S. Bunch, *Nat. Nano* **2011**, *6*, 543–546.
[31] J. S. Bunch, M. L. Dunn, *Solid State Communications* **2012**, *152*, 1359–1364.

© 2013 WILEY-VCH Verlag GmbH & Co. KGaA, Weinheim

[32] K. Das, R. C. Batra, *Smart Materials and Structures* **2009**, *18*, 115008.
[33] B. E. Artz, L. W. Cathey, *Solid-State Sensor and Actuator Workshop, 1992*. 5th Technical Digest., IEEE **1992**, 190–193.
[34] P. Osterberg, H. Yie, X. Cai, J. White, S. Senturia, *Micro Electro Mechanical Systems, 1994, MEMS '94, Proceedings*, IEEE Workshop on **1994**, 28–32.
[35] P. R. Gray, *Analysis and Design of Analog Integrated Circuits*, Wiley, **2009**.
[36] C. S. Ruiz-Vargas, H. L. Zhuang, P. Y. Huang, A. M. van der Zande, S. Garg, P. L. McEuen, D. A. Muller, R. G. Hennig, J. Park, *Nano Lett.* **2011**, *11*, 2259–2263.
[37] H. C. Nathanson, W. E. Newell, R. A. Wickstrom, J. R. Davis Jr., *Electron Devices, IEEE Transactions* on **1967**, *14*, 117–133.
[38] X. Liu, N. G. Boddeti, M. R. Szpunar, L. Wang, M. A. Rodriguez, R. Long, J. Xiao, M. L. Dunn, J. S. Bunch, *Nano Lett.* **2013**, *13*, 2309–2313.

© 2013 WILEY-VCH Verlag GmbH & Co. KGaA, Weinheim
Adv. Mater. **2013**,
DOI: 10.1002/adma.201304949